Microstructure and velocity of field-driven solid-on-solid interfaces moving under stochastic dynamics with local energy barriers

G. M. Buendía,[1,2,*] P. A. Rikvold,[2,3,4,†] and M. Kolesik[5,6,‡]
[1]*Department of Physics, Universidad Simón Bolívar, Caracas 1080, Venezuela*
[2]*School of Computational Science, Florida State University, Tallahassee, Florida 32306-4120, USA*
[3]*Center for Materials Research and Technology and Department of Physics, Florida State University, Tallahassee, Florida 32306-4350, USA*
[4]*National High Magnetic Field Laboratory, Tallahassee, Florida 32310, USA*
[5]*Institute of Physics, Slovak Academy of Sciences, Bratislava, Slovak Republic*
[6]*Optical Sciences Center, University of Arizona, Tucson, Arizona 85721, USA*
(Received 8 September 2005; revised manuscript received 12 December 2005; published 31 January 2006)

We study the microscopic structure and the stationary propagation velocity of (1+1)-dimensional solid-on-solid interfaces in an Ising lattice-gas model, which are driven far from equilibrium by an applied force, such as a magnetic field or a difference in (electro)chemical potential. We use an analytic nonlinear-response approximation [P. A. Rikvold and M. Kolesik, J. Stat. Phys. **100**, 377 (2000)] together with kinetic Monte Carlo simulations. Here we consider interfaces that move under Arrhenius dynamics, which include a microscopic energy barrier between the allowed Ising or lattice-gas states. Two different dynamics are studied: the standard one-step dynamics (OSD) [H. C. Kang and W. Weinberg, J. Chem. Phys. **90**, 2824 (1992)] and the two-step transition-dynamics approximation (TDA) [T. Ala-Nissila, J. Kjoll, and S. C. Ying, Phys. Rev. B **46**, 846 (1992)]. In the OSD the effects of the applied force and the interaction energies in the model factorize in the transition rates (soft dynamics), while in the TDA such factorization is not possible (hard dynamics). In full agreement with previous general theoretical results we find that the local interface width under the TDA increases dramatically with the applied force. In contrast, the interface structure with the OSD is only weakly influenced by the force, in qualitative agreement with the theoretical expectations. Results are also obtained for the force dependence and anisotropy of the interface velocity, which also show differences in good agreement with the theoretical expectations for the differences between soft and hard dynamics. Our results confirm that different stochastic interface dynamics that all obey detailed balance and the same conservation laws nevertheless can lead to radically different interface responses to an applied force.

DOI: 10.1103/PhysRevB.73.045437 PACS number(s): 68.35.Ct, 75.60.Jk, 68.43.Hn, 05.10.Ln

I. INTRODUCTION

To understand the properties of materials one has to understand surfaces and interfaces: materials interact with their environment through their surfaces, and material properties are profoundly influenced by internal interfaces. Processes related to surfaces and interfaces therefore play a critical role in nature and in a variety of technological applications, such as electronic, magnetic, and optical devices, sensors, catalysts, coatings, and many other industrial systems and processes.[1,2] Surfaces also play a vital role in biology and medicine, since most biological reactions occur at surfaces and interfaces. The applications of surface science in medicine range from the growth of biocompatible surfaces for tissue cultures, through medical implants, to the design of innumerable medical devices.[3,4] It is therefore crucial to understand the fundamental processes occurring at surfaces and interfaces in order to provide means of controlling and manipulating such systems. The large-scale properties of growing interfaces have been the object of an enormous amount of work in recent years,[5,6] but much less attention has been paid to interfacial structure on a microscopic scale. This is unfortunate because many important interface properties, such as mobility and catalytic and chemical activity, are largely determined by the microscopic interface structure. The microscopic structure limits the interfacial propagation velocity under an external driving force, such as an external field for a magnetic or dielectric domain wall, or a difference in chemical potential between the bulk phases for a crystal surface.

Since the detailed microscopic mechanism of the interface motion is often not known, one standard way to gain insight into the process is by constructing a stochastic model that mimics its essential features. Dynamics that conserve the order parameter, or ones that do not, must be chosen according to the physical characteristics of the system. Once this is decided, there are several dynamics in each category to choose among. It is well established that structures arising from different dynamics that obey detailed balance and respect the same conservation laws exhibit universal asymptotic large-scale features. However, recent studies[7–10] show that there are important differences between the *microstructures* of field-driven interfaces obtained with different dynamics and that these differences very significantly influence important interface properties such as mobility. A mean-field, nonlinear-response theory developed in Refs. 7 and 8 indicates that there are two different classes of nonconservative dynamics that lead to significantly different surface microstructures. These are the *soft* dynamics, in which the single-site transition rates can be factorized into one part that

depends only on the applied force and a second part that depends only on the interaction energies, and the *hard* dynamics, for which this factorization is not possible.[11] By this classification, the widely used Glauber and Metropolis dynamics are hard. Soft dynamics are appropriate for solidification or adsorption problems where the driving force is a chemical-potential difference.[12,13]

In previous papers[7,8] two of us introduced a dynamic mean-field approximation for the microstructure, based on the Burton-Cabrera-Frank solid-on-solid (SOS) approximation.[14] For soft dynamics, interface structures should remain independent of the applied force, while there should be a clear dependence on the force for hard dynamics. Monte Carlo (MC) simulation results with soft Glauber[8] and standard hard Glauber dynamics[8–10] confirm these predictions. Moreover, SOS surfaces generated with hard Glauber dynamics exhibit a skewness that is absent for soft Glauber dynamics. Since the mean-field results depend on the absence of short-range correlations along the interfaces, it remains an open question as to which extent these characteristics are shared by all soft and hard dynamics.

For the present study we have considered two dynamics that include a local energy barrier representing a transition state inserted between individual Ising or lattice-gas states. Such Arrhenius dynamics, as they are often called, are appropriate in kinetic MC simulations of discrete Ising or lattice-gas models in which the discrete states serve as approximations for high-probability configurations in an underlying continuous potential.[15,16] Examples are the study of diffusion in a lattice-gas model in a continuous corrugation potential,[17] the relaxation process from the high-spin state of molecular bistable solids,[18–20] or the approximation of a continuous spin model with strong uniaxial anisotropy by an Ising model.[21,22] When applied to kinetic Ising lattice-gas models, Arrhenius dynamics give nucleation rates quite different from the ones given by the standard Glauber dynamics,[23] another warning about the importance of choosing the right dynamics for specific physical or chemical systems.

The two Arrhenius dynamics that we consider here are the common one-step-dynamics[24,25] (OSD) and the two-step transition dynamic approximation[16,26] (TDA). The OSD dynamics are soft and the TDA dynamics are hard, according to the definitions given above. Their transition rates are defined in Sec. II. The OSD dynamics are commonly used in studies of adsorption, such as the electrosorption of halides on single-crystal silver electrodes.[27–29] Among the experimental systems that have been described with the TDA dynamics are the diffusion of H atoms on single-crystal tungsten surfaces.[26]

SOS surfaces belong to the Kardar-Parisi-Zhang (KPZ) dynamic universality class,[5,30] in which the macroscopic, stationary distribution for flat, moving interfaces is Gaussian, corresponding to a random walk with independent increments. Nevertheless, the step heights in several discrete models in this class are correlated at *short* distances.[31,32] In the mean-field approximation used here, these short-range correlations are ignored. The resulting discrepancies will be apparent when we compare the theoretical results with kinetic MC simulations.

The remainder of this paper is organized as follows. In Sec. II we introduce the SOS interface model and give the transition rates for the TDA and OSD dynamics. In Sec. III we summarize the mean-field approximation for the time evolution of the single-step probability density function (PDF), as well as its stationary form. We also give expressions for the class populations and interface velocity in terms of the applied force, the temperature, and the angle of the interface relative to the lattice axes. In Sec. IV we compare simulations and analytical predictions for the detailed stationary interface structure, including the asymmetry of the simulated nonequilibrium interfaces. A summary and conclusion are provided in Sec. V.

II. MODEL AND DYNAMICS

The SOS interfaces are described by the nearest-neighbor $S=1/2$ Ising Hamiltonian with anisotropic, ferromagnetic interactions J_x and J_y in the x and y directions, respectively:

$$\mathcal{H} = -\sum_{x,y} s_{x,y}(J_x s_{x+1,y} + J_y s_{x,y+1} + H), \tag{1}$$

where $s_{x,y}=\pm 1$, $\Sigma_{x,y}$ runs over all sites, and the applied field H is the driving force. The interface is introduced by fixing $s_{x,y}=+1$ and -1 for large negative and positive y, respectively. Without loss of generality we take $H \geqslant 0$, such that the interface on average moves in the positive y direction. This Ising model is equivalent to a lattice-gas model with local occupation variables $c_{x,y} \in \{0,1\}$.[33,34] Specifically, we identify $s=+1$ with $c=1$ (occupied or "solid") and $s=-1$ with $c=0$ (empty or "fluid"). The interactions in the Ising model, J_α, are related to the ones in the lattice-gas model, ϕ_α, as $J_\alpha=\phi_\alpha/4$, and the applied field is related to the lattice-gas chemical potential μ as $H=(\mu-\mu_0)/2$, where $\mu_0=-4(J_x+J_y)=-(\phi_x+\phi_y)$ is the coexistence value of μ. Here we will use Ising or lattice-gas language interchangeably as we feel it makes a particular aspect of the discussion clearer.

The SOS model considers an interface in a lattice-gas or $S=1/2$ Ising system on a square lattice of unit lattice constant as a single-valued integer function $h(x)$ of the x coordinate, with steps $\delta(x)=h(x+1/2)-h(x-1/2)$ at integer values of x. A typical SOS interface configuration is shown in Fig. 1. In this paper the two possible states of the site (x,y) are denoted by the two "spin" values $s_{x,y}=\pm 1$. (In order that the step positions and the interface heights be integer as stated above, we place the spins at odd half-integer values of x and y—i.e., at the centers of the unit cells separated by dotted lines in Fig. 1.)

The interface will be made to evolve under two different dynamics that contain a microscopic energy barrier against individual spin flips. These are the TDA[16,26] and the OSD.[24,25] The barrier represents a transition state which is inserted between the states allowed in the Hamiltonian, such as a saddle point in a corrugation potential for particle diffusion[15,17,26] or a high energy associated with a transitional spin state that is not along one of the two directions allowed by the Ising Hamiltonian.[21,22]

Here we express the transition-state energy by the approximation[16,24–26]

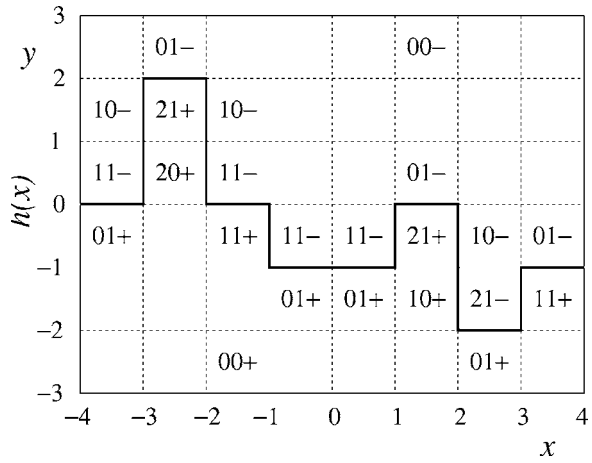

FIG. 1. A short segment of an SOS interface $y=h(x)$ between a positively magnetized phase (or "solid" phase in the lattice-gas picture) below and a negative (or "fluid") phase above. The step heights are $\delta(x)=h(x+1/2)-h(x-1/2)$. Interface sites representative of the different SOS spin classes (see Tables I and II) are marked with the notation *jks* explained in the text. Sites in the uniform bulk phases are 00− and 00+. This interface was randomly generated with a symmetric step-height distribution, corresponding to $\phi=0$. From Ref. 8.

$$E_T = \frac{E_i + E_f}{2} + U, \tag{2}$$

where E_i and E_f are the initial and final energies and U is the bare, microscopic energy barrier. In electrochemical applications, such as electron- or ion-transfer reactions, this corresponds to the symmetric Butler-Volmer approximation.[35] The construction corresponding to Eq. (2) is illustrated in Fig. 2.

Both the TDA and OSD are single-spin-flip (nonconservative) dynamics that satisfy detailed balance. This ensures the approach to equilibrium, which in this case is a uniformly positive phase with the interface pushed off to positive infinity. Such dynamics are defined by a single-spin transition rate $W(s_{x,y}\rightarrow -s_{x,y})=W(\beta\Delta E,\beta U)$. Here β is the inverse of the temperature T (Boltzmann's constant is taken as unity), $\Delta E = E_f - E_i$ is the energy change corresponding to a successful

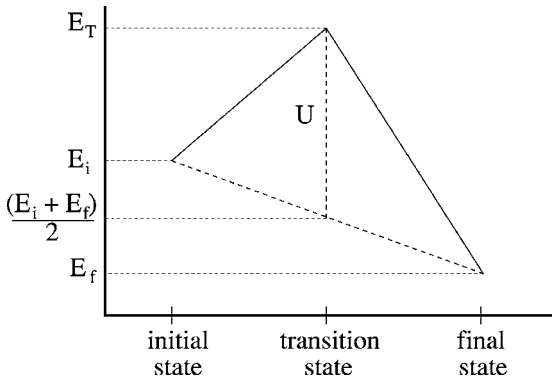

FIG. 2. Schematic picture of the transition barrier in the symmetric Butler-Volmer approximation, used to calculate the TDA and OSD transition rates. After Ref. 23.

spin flip, and U determines the energy barrier between the two states through Eq. (2). The detailed-balance condition (valid for transitions between allowed states) is expressed as $W(\beta\Delta E,\beta U)/W(-\beta\Delta E,\beta U)=e^{-\beta\Delta E}$, where the right-hand side is independent of U.

The transition rates for the TDA and OSD dynamics with the transition-state energy E_T given by Eq. (2) are defined as[16,17,26]

$$W_{\mathrm{TDA}} = \frac{1}{1+\exp[\beta(E_T-E_i)]}\frac{1}{1+\exp[\beta(E_f-E_T)]} \tag{3}$$

and[24,25]

$$W_{\mathrm{OSD}} = \exp[-\beta(E_T-E_i)] = \exp(-\beta U)\exp[-\beta\Delta E/2], \tag{4}$$

respectively.

Notice that the TDA transition rate cannot be factorized into one part that depends only on the interaction energy and another that depends only on the applied field; thus, it belongs to the class of dynamics defined as hard.[11] The OSD dynamics can be factorized this way and thus is classified as soft.[11] Another important difference between the TDA and OSD is that W_{TDA} is restricted to be between 0 and 1, while there is no upper bound on W_{OSD}. As a consequence, the same difference is observed for the propagation velocities. One may, however, question the physical realism of cases in which the transition-state energy E_T is below the initial energy E_i so that $W_{\mathrm{OSD}}>1$. In order to preserve the SOS configuration at all times, flips are allowed only at sites which have exactly one broken bond in the y direction.

With the Ising Hamiltonian there are only a finite number of different values of ΔE. The spins can therefore be divided into classes,[36–39] labeled by the spin value s and the number of broken bonds between the spin and its nearest neighbors in the x and y directions, j and k, respectively. The ten spin classes consistent with the SOS model are denoted *jks* with $j\in\{0,1,2\}$ and $k\in\{0,1\}$. They are shown in Fig. 1 and listed in Table I.

In the SOS model the heights of the individual steps are assumed to be statistically independent and identically distributed. The step-height probability density function (PDF) is given by the interaction energy corresponding to the $|\delta(x)|$ broken J_x bonds between spins in the columns centered at $(x-1/2)$ and $(x+1/2)$ as

$$p[\delta(x)] = Z(\phi)^{-1}X^{|\delta(x)|}e^{\gamma(\phi)\delta(x)}. \tag{5}$$

The factor X determines the width of the PDF, and $\gamma(\phi)$ is a Lagrange multiplier which maintains the mean step height at an x-independent value, $\langle\delta(x)\rangle=\tan\phi$, where ϕ is the overall angle between the interface and x axis. In equilibrium, X is simply the Boltzmann factor $e^{-2\beta J_x}$. The partition function is

$$Z(\phi) = \sum_{\delta=-\infty}^{+\infty} X^{|\delta|}e^{\gamma(\phi)\delta} = \frac{1-X^2}{1-2X\cosh\gamma(\phi)+X^2}, \tag{6}$$

where $\gamma(\phi)$ is given by

TABLE I. The spin classes in the anisotropic square-lattice SOS model. The first column contains the class labels *jks*. The second column contains the total field and interaction energy for a spin in each class, $E(jks)$, relative to the energy of the state with all spins parallel and $H=0$, $E_0=-2(J_x+J_y)$. The third column contains the change in the total system energy resulting from reversal of a spin from s to $-s$, $\Delta E(jks)$. The fourth and fifth columns contain E_T-E_i and E_f-E_T, respectively. The first three classes have nonzero populations in the SOS model, and flipping a spin in any of them preserves the SOS configuration. The other two classes (marked †) also have nonzero populations in the SOS model, but flipping a spin in any of them would produce an overhang or a bubble and is therefore forbidden. Note that in this table, s represents the spin value *before* the spin flip.

Class, *jks*	$E(jks)-E_0$	$\Delta E(jks)$	E_T-E_i	E_f-E_T
$01s$	$-sH+2J_y$	$2sH+4J_x$	$sH+2J_x+U$	$sH+2J_x-U$
$11s$	$-sH+2(J_x+J_y)$	$2sH$	$sH+U$	$sH-U$
$21s$	$-sH+2(2J_x+J_y)$	$2sH-4J_x$	$sH-2J_x+U$	$sH-2J_x-U$
$10s$ †	$-sH+2J_x$	$2sH+4J_y$	$sH+2J_y+U$	$sH+2J_y-U$
$20s$ †	$-sH+4J_x$	$2sH-4(J_x-J_y)$	$sH-2(J_x-J_y)+U$	$sH-2(J_x-J_y)-U$

$$e^{\gamma(\phi)}=\frac{(1+X^2)\tan\phi+[(1-X^2)^2\tan^2\phi+4X^2]^{1/2}}{2X(1+\tan\phi)} \quad (7)$$

(see details in Refs. 7 and 8). Simple results are obtained for $\phi=0$, which yields $\gamma(0)=0$ and

$$Z(0)=(1+X)/(1-X), \quad (8)$$

and for $\phi=45^\circ$ (see Ref. 8).

The mean spin-class populations $\langle n(jks)\rangle$ are all obtained from the product of the independent PDF's for $\delta(x)$ and $\delta(x+1)$. Symmetry of $p[\delta(x)]$ under the transformation $(x,\phi,\delta)\to(-x,-\phi,-\delta)$ ensures that $\langle n(jk-)\rangle=\langle n(jk+)\rangle$ for all j and k. Numerical results illustrating the breakdown of this up-down symmetry for large H are discussed in Sec. IV. The general expressions for the class populations are given in the second column of Table II; details of the calculation can be found in Ref. 7. The results for each of the dynamics are obtained by substituting their respective values of X, which will be calculated in the next Section.

Whenever a spin at the interface flips from -1 to $+1$, the corresponding column of the interface advances by one lattice constant in the y direction. Conversely, a column (not necessarily the same one) recedes by one lattice constant when a spin at the interface flips from $+1$ to -1. The mean velocity of the interface in the y direction, $\langle v_y\rangle$, is the difference between the rates of forward and backward steps, averaged over the whole interface. The energy changes corresponding to the flips are given in the third column in Table I. The sum over x that gives the average velocity can be rearranged into a sum over the spin classes of transition rates, weighted by the average class populations. Since the spin-class populations on both sides of the interface are equal in this approximation, the contribution to $\langle v_y\rangle$ from sites in the classes $jk-$ and $jk+$ therefore becomes

$$\langle v_y(jk)\rangle=W(\beta\Delta E(jk-),\beta U)-W(\beta\Delta E(jk+),\beta U). \quad (9)$$

The mean propagation velocity perpendicular to the interface becomes

$$\langle v_\perp(T,H,\phi)\rangle=\cos(\phi)\langle v_y\rangle=\cos(\phi)\sum_{j,k}\langle n(jks)\rangle\langle v_y(jk)\rangle, \quad (10)$$

where the sum runs over the classes included in Table II. It has been shown in Ref. 7 that Eq. (10) reduces to the results for the single-step[36,40–42] and polynuclear growth[40,43,44] models at low temperatures for large and small ϕ, respectively.

III. NONLINEAR RESPONSE

With $X=e^{-2\beta J_x}$—i.e., independent of H—the results in Table II correspond to a linear-response approximation for the velocity. In previous papers[7,8] an expression for a field-

TABLE II. The mean populations for the spin classes of the SOS interface, with the corresponding contributions to the interface velocity under the TDA and OSD dynamics. The first column contains the class labels *jks*. The second column contains the mean spin-class populations for general tilt angle ϕ, with $\cosh\gamma(\phi)$ from Eq. (7). The third and fourth columns contain the contributions to the mean interface velocity in the y direction from spins in classes $jk-$ and $jk+$, Eq. (9), using the SOS-preserving TDA and OSD dynamics, respectively. For the TDA dynamics, $X=X(T,H)$ is given by Eq. (12), and for the OSD dynamics, X is independent of H and is given by Eq. (13). In the third column $A=[\cosh(2\beta J_x)\cosh(\beta H)+\cosh(\beta U)]$ and $B=\sinh(2\beta J_x)\sinh(\beta H)$.

Class, *jks*	$\langle n(jks)\rangle$	$\langle v_y(jk)\rangle_{\mathrm{TDA}}$	$\langle v_y(jk)\rangle_{\mathrm{OSD}}$
$01s$	$[1-2X\cosh\gamma(\phi)+X^2]/(1-X^2)^2$	$e^{-2\beta J_x}[A\sinh(\beta H)+B\cosh(\beta H)]/[A^2-B^2]$	$e^{-\beta(U+2J_x)}2\sinh(\beta H)$
$11s$	$2X[(1+X^2)\cosh\gamma(\phi)-2X]/(1-X^2)^2$	$\sinh(\beta H)/[\cosh(\beta H)+\cosh(\beta U)]$	$e^{-\beta U}2\sinh(\beta H)$
$21s$	$X^2[1-2X\cosh\gamma(\phi)+X^2]/(1-X^2)^2$	$e^{2\beta J_x}[A\sinh(\beta H)-B\cosh(\beta H)]/[A^2-B^2]$	$e^{-\beta(U-2J_x)}2\sinh(\beta H)$

dependent $X(T,H)$ was obtained, based on a dynamic mean-field approximation for the equation of motion for the single-step PDF together with a detailed-balance argument for the stationary state. This improved nonlinear response approximation gives (see Ref. 8 for details of the calculation)

$$X(T,H) = e^{-2\beta J_x}\left\{ \frac{e^{-2\beta H} W[\beta(-2H-4J_x),\beta U] + e^{2\beta H} W[\beta(2H-4J_x),\beta U]}{W[\beta(-2H-4J_x),\beta U] + W[\beta(2H-4J_x),\beta U]} \right\}^{1/2}, \tag{11}$$

which is independent of $\gamma(\phi)$. Here $W(\beta\Delta E,\beta U)$ are the transition rates associated with the reversal of a single spin. The values of ΔE, $E_T - E_i$, and $E_f - E_T$ are given in Table I for the different spin classes.

Equation (11) shows that $X(T,H)$ depends on the specific dynamics, except for $H=0$, where it reduces to its equilibrium value, $X(T,0)=e^{-2\beta J_x}$. It is easy to see from the equation that for soft dynamics, where the field and interaction contributions to the transition rates factorize, the H dependence in Eq. (11) cancels out. In Ref. 9 it was demonstrated that the soft Glauber dynamics yields an SOS interface that is identical to the equilibrium SOS interface at $H=0$ and the same temperature, regardless of the value of H. Hard dynamics, such as the standard Glauber and Metropolis dynamics and the TDA, lead to a nontrivial field dependence in X.

Inserting the transition rates corresponding to the TDA and OSD dynamics, defined by Eqs. (3) and (4), respectively, into Eq. (11), we explicitly get

$$X_{\mathrm{TDA}}(T,H) = e^{-2\beta J_x}\left\{ \frac{e^{2\beta J_x}\cosh(2\beta H) + e^{-2\beta J_x} + 2\cosh(\beta U)\cosh(\beta H)}{e^{-2\beta J_x}\cosh(2\beta H) + e^{2\beta J_x} + 2\cosh(\beta U)\cosh(\beta H)} \right\}^{1/2} \tag{12}$$

and

$$X_{\mathrm{OSD}}(T,H) = e^{-2\beta J_x} = X(T,0). \tag{13}$$

We note that X_{TDA} is similar, but not identical, to the one for the standard Glauber dynamics, Eq. (18) of Ref. 8. The spin-class populations listed in Table II can now be calculated explicitly for each of the dynamics by replacing X with its corresponding value. The expressions for the contributions to the mean velocity in the y direction, Eq. (9), for each class in the TDA and OSD dynamics are given in the third and fourth columns of Table II, respectively.

In the next section we show that the nonlinear-response approximation gives good agreement with MC simulations of driven, flat SOS interfaces evolving under the TDA and OSD dynamics for a wide range of fields and temperatures.

IV. COMPARISON WITH MONTE CARLO SIMULATIONS

We calculated the step-height distributions, propagation velocities, and spin-class populations, analytically and by kinetic MC simulations, for both the TDA and OSD dynamics in the isotropic case, $J_x=J_y=J$. The details of our particular implementation of the n-fold way, rejection-free MC algorithm[37,38] are essentially the same as described in Ref. 7, except for two points. The first is that only transitions from the classes with one broken y bond ($k=1$) are allowed, so as to preserve the SOS interface structure. The second difference is that the present code uses *continuous time*[45] to accommodate the large transition rates that are possible with the OSD dynamics. By keeping only the interface sites in memory, the algorithm is not subject to any size restriction in the y direction and simulations can be carried out for arbitrarily long times.

The numerical results presented here are based on MC simulations mostly at the two temperatures $T=0.2T_c$ and $0.6\,T_c$ [$T_c=-2J/\ln(\sqrt{2}-1)\approx 2.269J$ is the critical temperature for the isotropic, square-lattice Ising model[46]], with $L_x=10\,000$ and fixed ϕ between 0 and 45°. The microscopic transition barrier U [see Eq. (2)] is chosen to be $0.5J$. This is the same value used in a previous study of nucleation with the OSD and TDA dynamics.[23] From Eq. (4) it is clear that for the OSD dynamics U only appears in a temperature-dependent scaling factor in the transition rate. It thus has no influence on the interface structure. For the TDA dynamics, on the other hand, an increase in U leads to a decrease in the local interface width and consequently in the propagation velocity. Also, the observed skewness increases, suggesting increasing short-range correlations between the step heights. These results are discussed in detail in a separate paper.[47]

In order to ensure stationarity we ran the simulation for 50 000 n-fold way updates per updatable spin (UPS) before taking any measurements. Stationary class populations and interface velocities were averaged over 50 000 UPS. For the stronger fields at $T=0.2T_c$ we used 10 times as many UPS. Adequate statistics for one- and two-step PDF's were ensured by the large L_x.

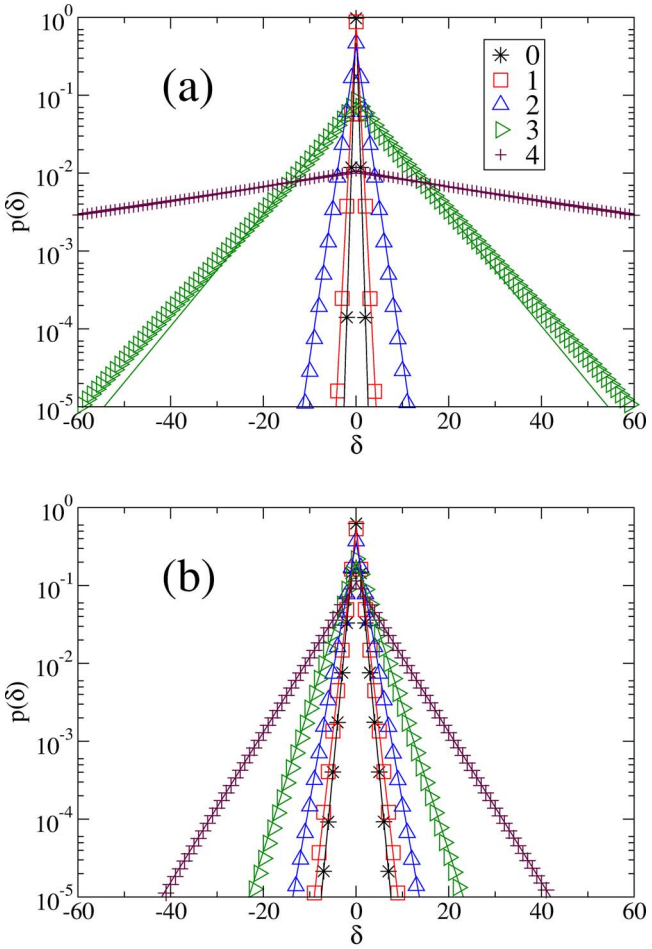

FIG. 3. (Color online) MC (data points) and analytical (solid lines) results for the stationary single-step PDF calculated with the TDA dynamics, shown on a logarithmic scale vs δ, for the values of H/J given in the legend. (a) $T=0.2T_c$. (b) $T=0.6T_c$. The symbols (and colors) have the same interpretations in (a) and (b).

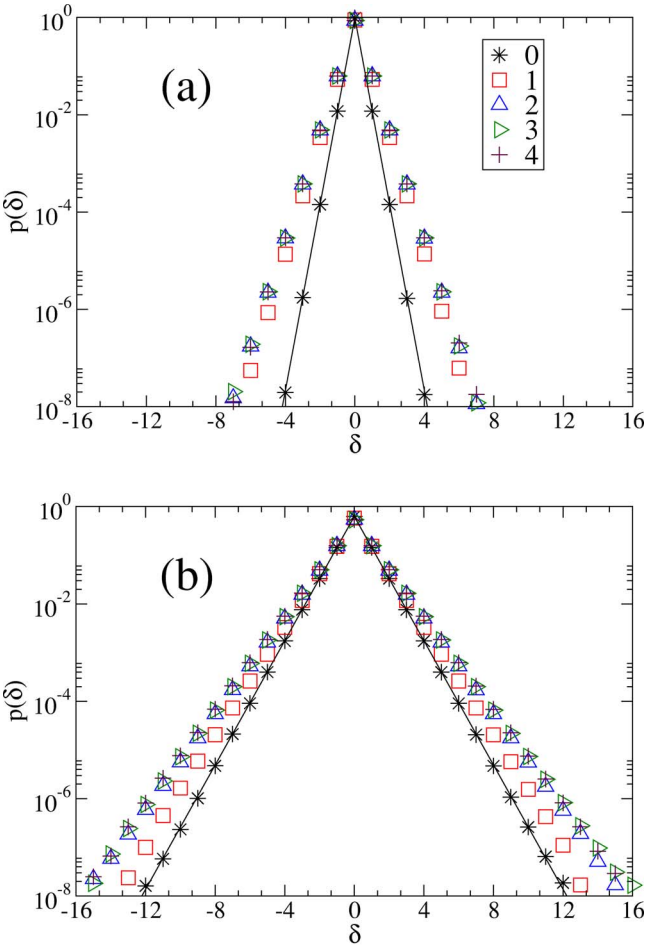

FIG. 4. (Color online) The stationary single-step PDF calculated with the OSD dynamics, shown on a logarithmic scale vs δ. The data points indicate MC results, and the straight lines are the theoretical predicted values (independent of H). The values of H/J are given in the legend. (a) $T=0.2T_c$. (b) $T=0.6T_c$. The symbols and colors have the same interpretations in (a) and (b). Note the very different scales from Fig. 3.

A. Stationary single-step probability densities

Stationary single-step PDF's were obtained by MC simulation at $T=0.2T_c$ and $0.6T_c$ for $\phi=0$ and several values of H. The simulation data and the theoretical results for $p[\delta]$ are shown in Figs. 3 and 4 for the TDA and OSD dynamics, respectively. The theoretical results are calculated with Eq. (5), with $X(T,H)$ from Eq. (12) for the TDA dynamics and from Eq. (13) for the OSD dynamics. For the TDA dynamics, Fig. 3, the agreement is excellent at the higher temperature for all the values of H analyzed (up to $H/J=4$). However, at the lower temperature the agreement is not very good for fields above $H/J=2.5$. For the OSD dynamics, Fig. 4 shows that, contrary to the theoretical mean-field results, $p(\delta)$ depends somewhat on H. This dependence is stronger for small fields and at the lower temperature. However, although not absent as expected from the mean-field approximation, the field dependence is *much weaker* than for the TDA dynamics.

Another way to compare the analytical and simulation results is by calculating $\langle|\delta|\rangle$ by summation of Eq. (5), $\langle|\delta|\rangle=2X/(1-X^2)$, with X from Eq. (12) for the TDA dynamics or X from Eq. (13) (independent of H) for the OSD, and comparing these values with the simulated ones. The simulation values for $\langle|\delta|\rangle$ can be obtained in two ways: directly by summation over the numerically obtained PDF and also from the probability of zero step height as $\langle|\delta|\rangle=\{p[0]^{-1}-p[0]\}/2$. This latter expression is obtained by observing that $p[0]=(1-X)/(1+X)$ for $\phi=0$, then solving this for X, and inserting the result into the above equation for $\langle|\delta|\rangle$ in terms of X. The results are shown in Fig. 5 for both dynamics, for $\phi=0$ at $T=0.2T_c$ and $0.6T_c$ calculated theoretically (solid lines) and by MC simulation (symbols). The agreement between the simulation and theoretical results for the TDA is excellent except at the low temperature, where for intermediate fields a slight deviation can be seen. The results are similar to those obtained with the standard Glauber dynamics. [See Fig. 5(a) of Ref. 8.] Again the results for the OSD dynamics show that, contrary to the theoretical prediction, there is a clear, albeit weak, dependence of the step height on the field. The theoretical and simulation results for the OSD dynamics only coincide at $H/J=0$.

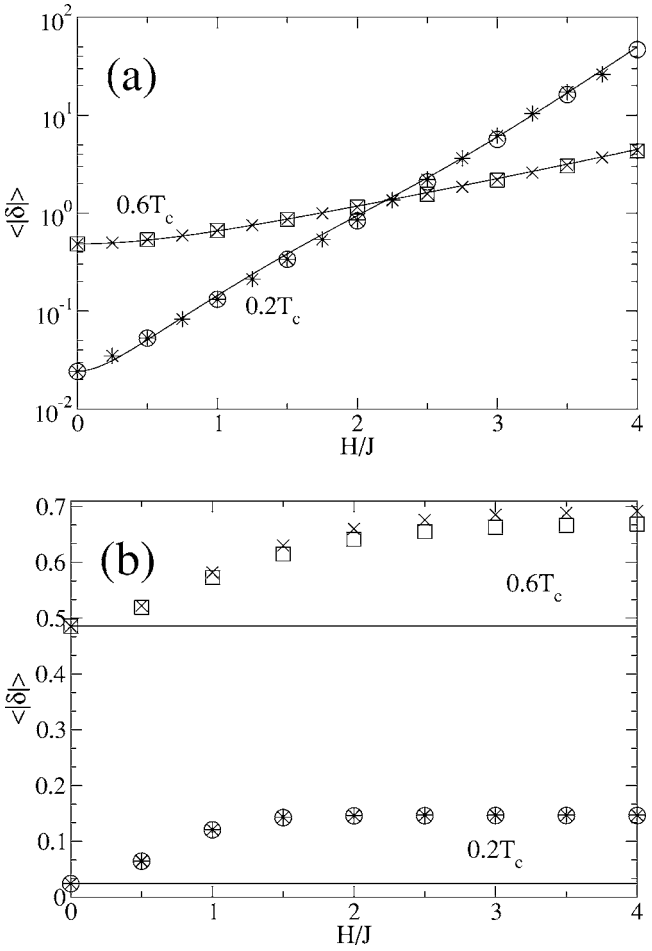

FIG. 5. Average stationary step height $\langle|\delta|\rangle$ vs H for $\phi=0$ at $T=0.2T_c$ and $0.6T_c$. The curves represent the theoretical results. The MC data were obtained directly by summation over the simulated single-step PDF's (asterisks and crosses) and from the probability of zero step height (circles and squares). See the text for details. Curve with circles and asterisks: $T=0.2T_c$. Curve with squares and crosses: $T=0.6T_c$. (a) TDA dynamics, shown on a logarithmic vertical scale. (b) OSD dynamics, shown on a linear vertical scale. In this and all the following figures, the statistical uncertainty is much smaller than the symbol size.

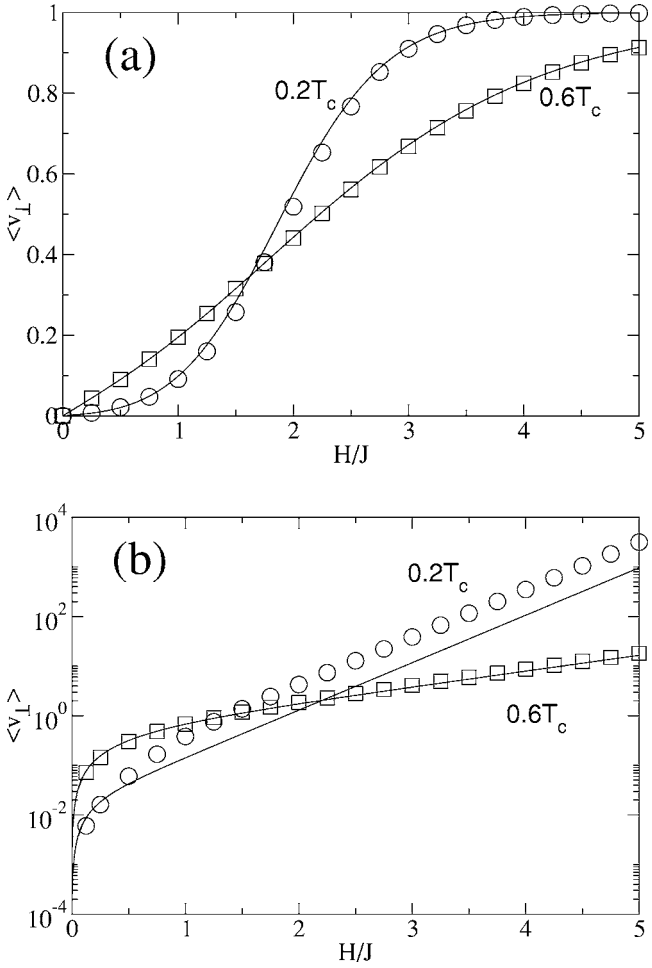

FIG. 6. The average stationary normal interface velocity $\langle v_\perp\rangle$ vs H for $\phi=0$. The MC results are shown as data points, circles for $T=0.2T_c$ and squares for $T=0.6T_c$, and the theoretical results as solid curves. (a) TDA, shown on a linear vertical scale. (b) OSD, shown on a logarithmic vertical scale.

The difference between the two dynamics is evident: the step heights for the OSD dynamics are weakly dependent on H, particularly for low values of H, in contrast with the very strong H dependence obtained for the TDA dynamics. This behavior is typical for differences expected between soft and hard dynamics.[9]

B. Stationary interface velocities

In this section we compare the interface velocities obtained for the TDA and OSD dynamics. In each case the velocities are calculated with the analytical approximation, Eq. (10), and by simulations. Figures 6(a) and 6(b) show the normal velocity versus H for $\phi=0$ for the TDA and OSD dynamics, respectively. There is excellent agreement between the MC results and the nonlinear-response theory for the TDA dynamics, except for a slight disagreement seen at $0.2T_c$ between $H/J=1.5$ and 2.5. The results are very similar to those obtained with the standard Glauber dynamics. (See Fig. 6 of Ref. 8.) However, for the OSD dynamics at the lower temperature, the nonlinear-response approximation underestimates the velocity, especially at higher fields. One of the main differences between the two dynamics is clearly seen in Fig. 6: the velocity is bounded by unity for the TDA while it increases exponentially with H for the OSD.

The dependence of the normal velocity on the tilt angle ϕ is shown in Figs. 7 and 8, for the TDA and OSD dynamics, respectively. We show results for several values of H/J at $T=0.2T_c$ and $T=0.6T_c$. For the TDA dynamics, the agreement between the theoretical results and simulations is excellent. The results are qualitatively similar to those obtained with the standard Glauber dynamics. (See Fig. 7 of Ref. 8.) For the OSD, the agreement between theory and simulation is excellent at the higher temperature. However, at the lower temperature and higher fields the agreement is only good at large values of ϕ.

In both cases it is seen that at $T=0.2T_c$ in weak fields the velocity increases with ϕ, in agreement with the polynuclear

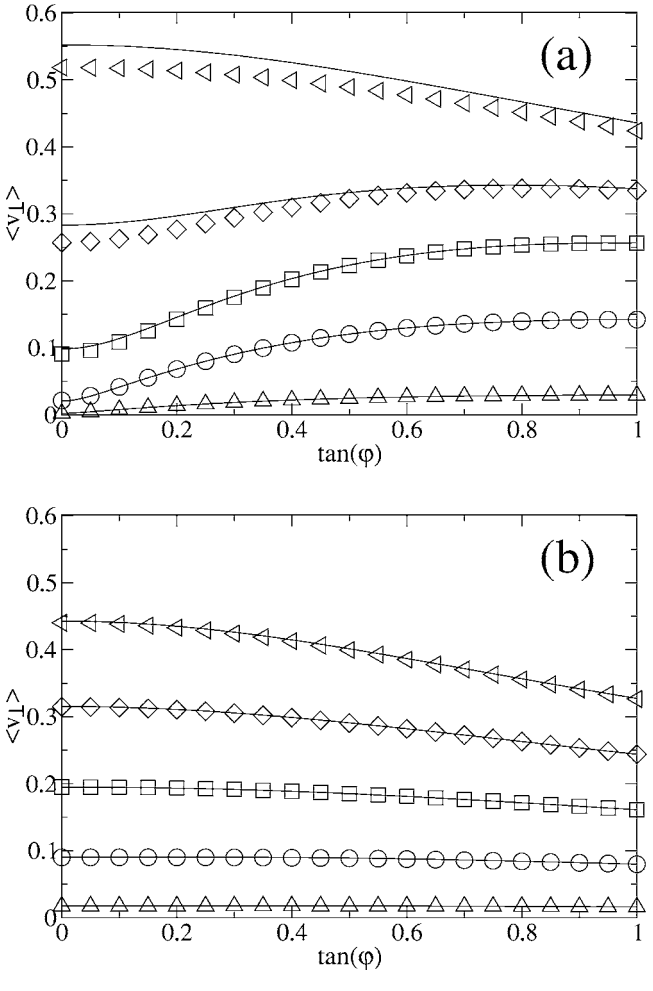

FIG. 7. The average stationary normal interface velocity $\langle v_\perp \rangle$ vs $\tan \phi$, calculated with the TDA dynamics, for $H/J=0.1$ (up triangles), 0.5 (circles), 1 (squares), 1.5 (diamonds), and 2.0 (left triangles). The symbols represent MC data and the solid curves analytical results. (a) $T=0.2T_c$. (b) $T=0.6T_c$.

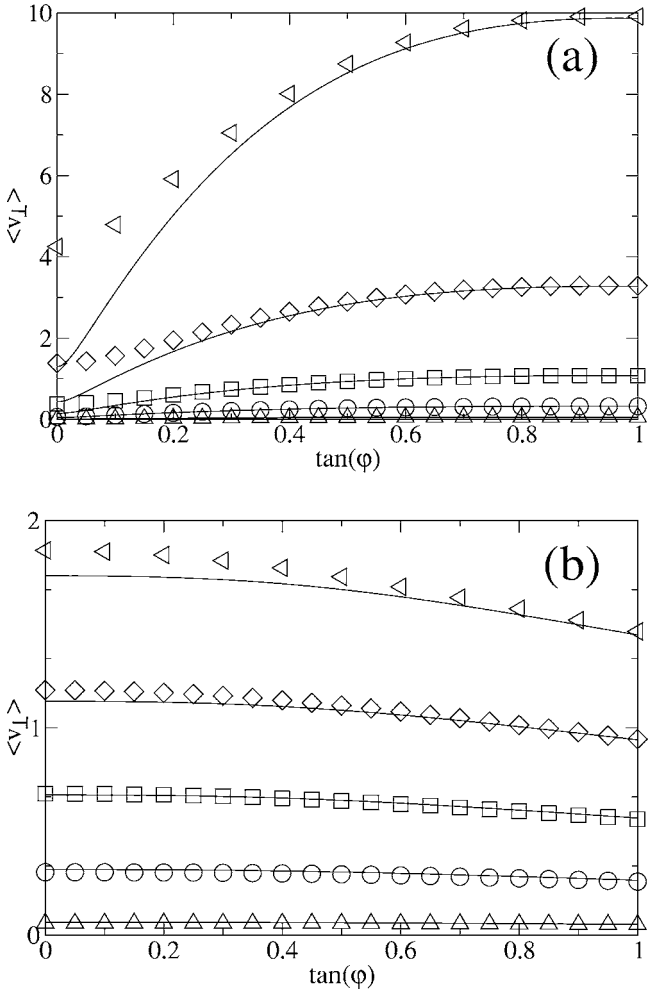

FIG. 8. The average stationary normal interface velocity $\langle v_\perp \rangle$ vs $\tan \phi$, calculated with the OSD dynamics, for $H/J=0.1$ (up triangles), 0.5 (circles), 1 (squares), 1.5 (diamonds), and 2.0 (left triangles). The symbols represent MC data and the solid curves analytical results. (a) $T=0.2T_c$. (b) $T=0.6T_c$. Note the difference in the vertical scales.

growth model at small angles and the single-step model for larger angles. However, for strong fields the TDA dynamics change gradually to the reverse anisotropy of Eden-type models.[48,49] No such change is observed for the OSD dynamic. At $T=0.6T_c$, on the other hand, both models behave very similarly. The velocity is nearly isotropic for weaker fields, while becoming Eden-like for stronger fields.

The temperature dependence of the normal interface velocity is shown in Fig. 9 for several values of H/J. For the TDA dynamics, Fig. 9(a), the agreement between the simulations and analytical results is excellent almost everywhere, except for a small discrepancy at intermediate T and H. This discrepancy is expected from the results shown in Fig. 6. This figure shows that at low T, the velocity changes steeply from zero to unity at some value between $H/J=2$ and $H/J=2.5$, developing a step discontinuity in H at $T=0$. The results are qualitatively similar to those obtained with the standard Glauber dynamics. (See Fig. 8 of Ref. 8.) For the OSD, Fig. 9(b), the theoretical and simulation results agree only when the temperature is higher than a minimum value that increases as the field increases. In this case the velocity also has a step discontinuity at $T=0$: for H/J below 1.5 the velocity goes to zero. For stronger fields the velocity at $T=0$ increases dramatically with H and decreases very rapidly as the temperature increases. As can be seen from Eq. (10) and Table II, the mean-field theory predicts that the contributions to the propagation velocity from each of the classes at low T is proportional to $\exp[-\beta(2J_x+U-H)]$. Thus, there is a discontinuity at $T=0$ for $H=2J_x+U$—i.e., for $H/J=2.5$ for our selection of $U=0.5J$. Beyond this value of H, the velocity diverges to infinity as $T\to 0$. Such a divergence at $T=0$ is not present for the soft Glauber dynamics, where the velocity vanishes at $T=0$ for all values of H.[10]

C. Spin-class populations and skewness

Since the analytical predictions for the class populations are based on the assumption that different steps are statistically independent, a comparison with the simulation results gives a way of testing this assumption. The six mean class

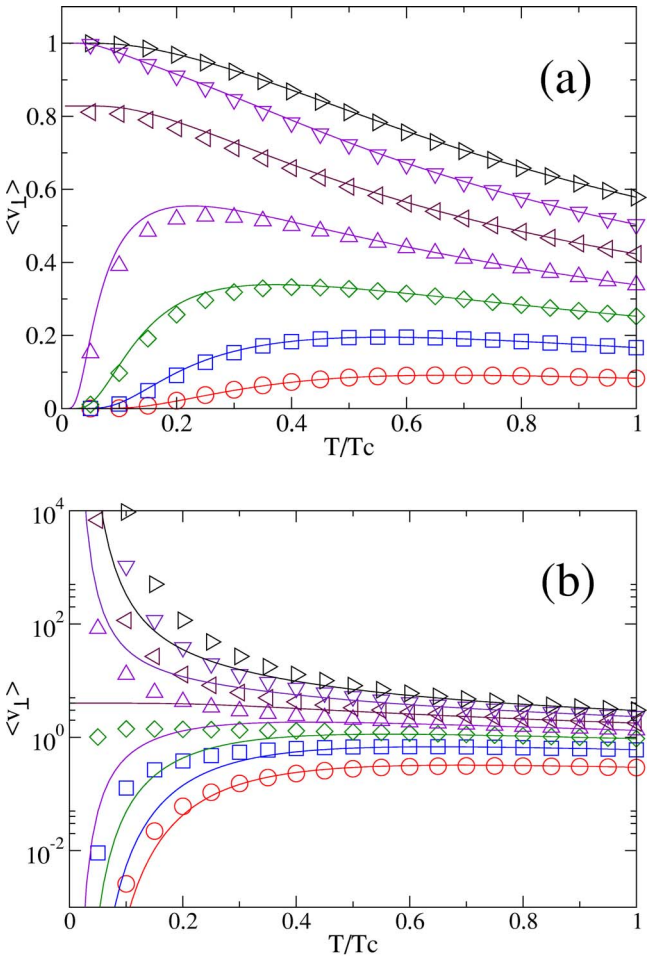

FIG. 9. (Color online) The average stationary normal interface velocity $\langle v_\perp \rangle$ vs T for $\phi=0$ and H/J between 0.5 and 3.5. MC data are represented by data points and analytical results by solid curves. From below to above, the values of H/J are 0.5 (circles), 1.0 (squares), 1.5 (diamonds), 2.0 (up triangles), 2.5 (left triangles), 3.0 (down triangles), and 3.5 (right triangles). Online, the colors of the curves and symbols match. (a) TDA, on a linear vertical scale. (b) OSD, on a logarithmic vertical scale.

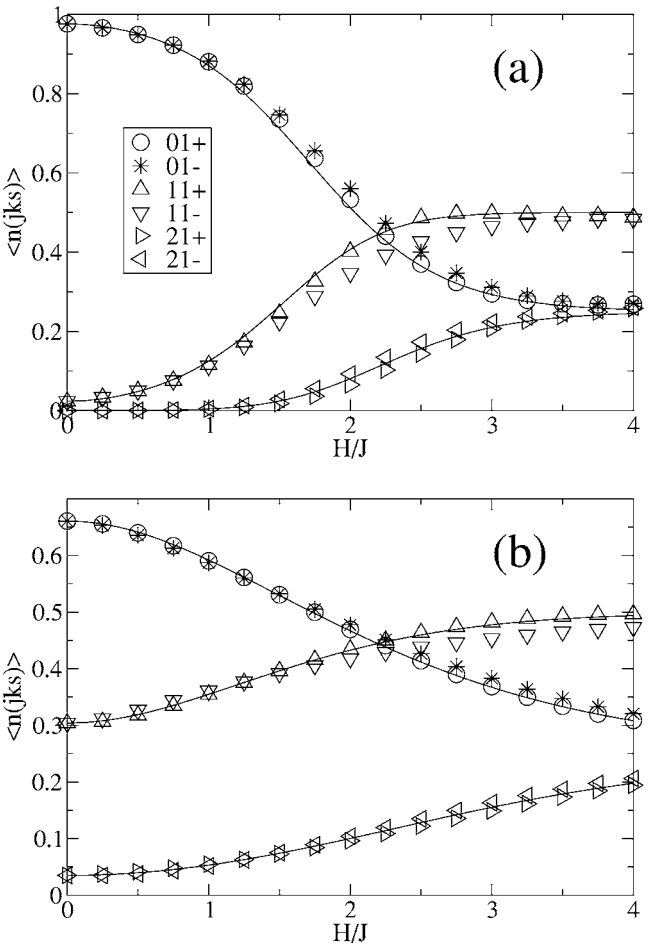

FIG. 10. Mean stationary class populations $\langle n(jks) \rangle$ vs H/J for $\phi=0$, calculated for the TDA dynamics. The simulation results are indicated by symbols and the analytic approximations by solid curves. (a) $T=0.2T_c$. (b) $T=0.6T_c$. The symbols have the same interpretations in (a) and (b). Note the different vertical scales in the two parts.

populations $\langle n(01s) \rangle$, $\langle n(11s) \rangle$, and $\langle n(21s) \rangle$ with $s=\pm 1$ – for $\phi=0$ at $T=0.2T_c$ and $0.6T_c$ are shown versus H in Figs. 10 and 11 for the TDA and the OSD dynamics, respectively. For the TDA at both temperatures, Fig. 10, the analytical approximations follow the average of the populations for $s=+1$ and $s=-1$ quite well. However, at intermediate fields the simulations show that the population in front of the surface ($s=-1$) is quite different from the one behind it ($s=+1$). The mean-field approximation seems to reproduce better the population behind the surface. The results are qualitatively similar to those obtained with the standard Glauber dynamics. (See Fig. 9 of Ref. 8.) For the OSD, Fig. 11, the mean-field approximation predicts that the mean class populations should be independent of H (since X is independent of H), while the simulation indicates a weak H dependence. For small fields there is a clear dependence of the population on the field, but as the field increases, the populations tend to fixed values independent of the field. The H dependence is consistent with the results for $\langle |\delta| \rangle$ and $X(T,H)$, shown in Fig. 5(b).

The short-range correlations between neighboring steps are responsible for the skewness between the spin populations on the leading and trailing edges of the interface that appears in the simulation results. This phenomenon is commonly observed in driven interfaces. It occurs even when the *long-range* correlations vanish as they do for interfaces in the KPZ dynamic universality class, to which the present models belong for all finite, nonzero values of H. Skewness has also been observed in several other SOS-type models, such as the body-centered SOS model studied by Neergaard and den Nijs,[31] the model for step propagation on crystal surfaces with a kink-Ehrlich-Schwoebel barrier studied by Pierre-Louis *et al.*,[50] and a model for the local time horizon in parallel kinetic MC simulations studied by Korniss *et al.*[32] No skewness was observed for the SOS model with the soft Glauber dynamics.[9] However, a small skewness was observed for the Ising model (whose interfaces include bubbles and overhangs) with soft Glauber dynamics (about two orders of magnitude smaller than the skewness observed for

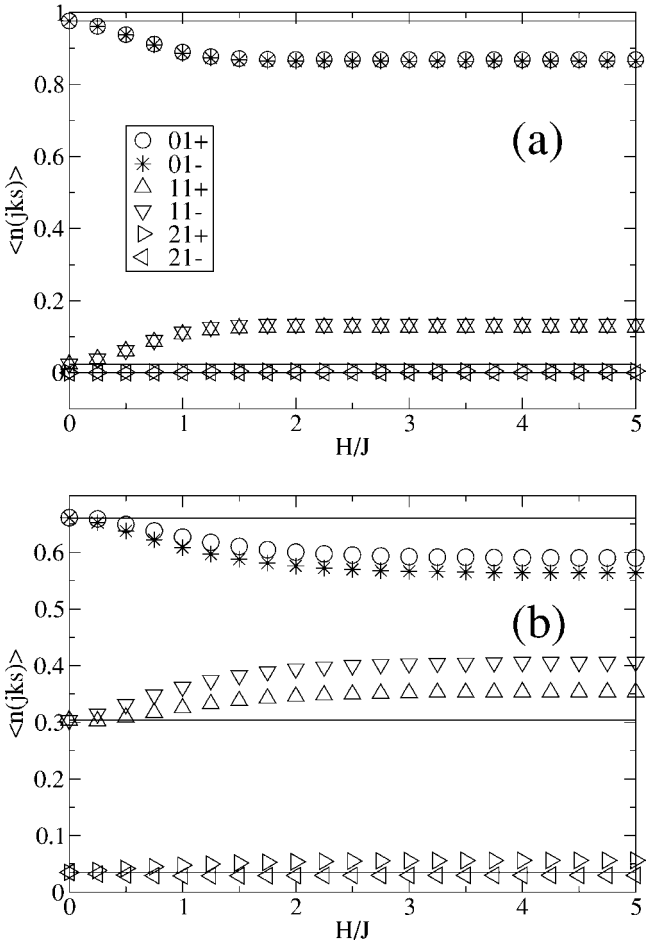

FIG. 11. Mean stationary class populations $\langle n(jks)\rangle$ vs H/J for $\phi=0$ calculated for the OSD dynamics. The simulation results are indicated by the symbols, and the straight lines indicate the theoretical predicted values (independent of H). (a) $T=0.2T_c$. (b) $T=0.6T_c$. The symbols have the same interpretations in (a) and (b). Note the different vertical scales in the two parts.

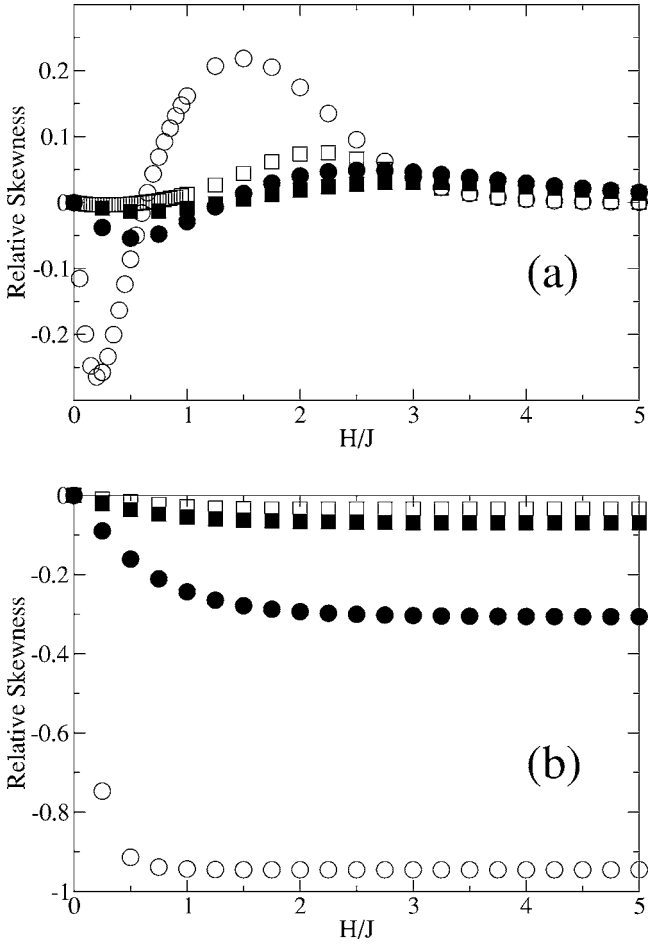

FIG. 12. The two relative skewness parameters ρ (circles) and ϵ (squares), defined in Eqs. (14) and (15), respectively. The parameters are shown vs H for $\phi=0$, at $T=0.2T_c$ (open symbols) and at $T=0.6T_c$ (solid symbols). (a) TDA. (b) OSD. Note the different vertical scales in the two parts.

the hard Glauber dynamics).[10] The correlations associated with the skewness generally lead to a broadening of protrusions on the leading edge ("hilltops"), while those on the trailing edge ("valley bottoms") are sharpened,[31] or the other way around.[32] In terms of spin-class populations, the former corresponds to $\langle n(21-)\rangle > \langle n(21+)\rangle$ and $\langle n(11+)\rangle > \langle n(11-)\rangle$. The relative skewness can therefore be quantified by the two functions[31]

$$\rho = \frac{\langle n(21-)\rangle - \langle n(21+)\rangle}{\langle n(21-)\rangle + \langle n(21+)\rangle} \tag{14}$$

and[8]

$$\epsilon = \frac{\langle n(11+)\rangle - \langle n(11-)\rangle}{\langle n(11+)\rangle + \langle n(11-)\rangle}. \tag{15}$$

These two skewness parameters are shown together in Fig. 12(a) for the TDA and in Fig. 12(b) for the OSD. For both dynamics the relative skewness is seen to be considerably stronger at the lower temperature. The temperature dependence is especially pronounced for ρ, due to the low concentration of sites in the class $21+$ at low temperatures. The OSD results contrast with previous results that showed that an SOS interface with soft Glauber dynamics does not present skewness.[9] In the present case, the SOS interface evolving under the soft OSD dynamics presents stronger relative skewness at lower temperature than the one evolving under the hard TDA dynamics.

Another way to visualize the skewness is to consider the joint two-step PDF $p[\delta(x), \delta(x+1)]$. Logarithmic contour plots of this quantity for both dynamics at different values of H, for $\phi=0$ at $T=0.6T_c$, are shown in Figs. 13 and 14. It is clearly seen that in both dynamics the contours change with H. For $H=0$ a symmetric diamond shape with equidistant contours indicates statistical independence with single-step PDF's given by Eq. (5). This equilibrium result is correctly observed in both the TDA dynamics, Fig. 13(a), and the OSD dynamics, Fig. 14(a). However, for nonzero fields the dynamics show different behavior. For the TDA, at stronger fields, the shapes are convex in the second quadrant $[\delta(x) < 0, \delta(x+1) > 0]$, Figs. 13(c) and 13(d). This shape indicates that large negative $\delta(x)$ tend to be followed by large positive

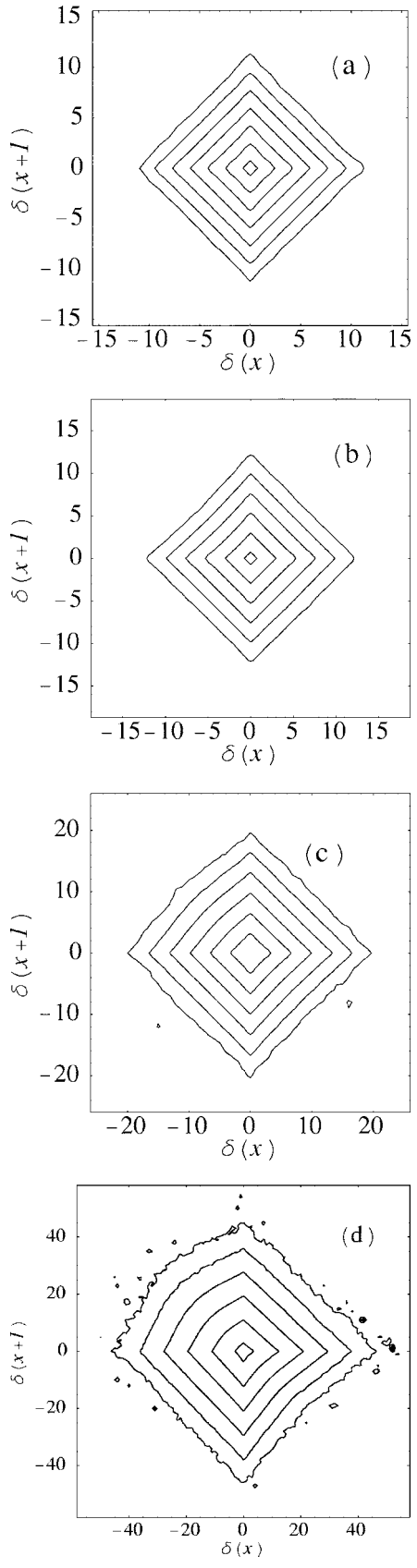

FIG. 13. Contour plots of $\log_{10}p[\delta(x),\delta(x+1)]$ for $\phi=0$ at $T=0.6T_c$ for the TDA dynamics. (a) $H/J=0$. (b) $H/J=1.0$. (c) $H/J=2.0$. (d) $H/J=3.5$. Note the different scales in the four parts. See discussion in the text.

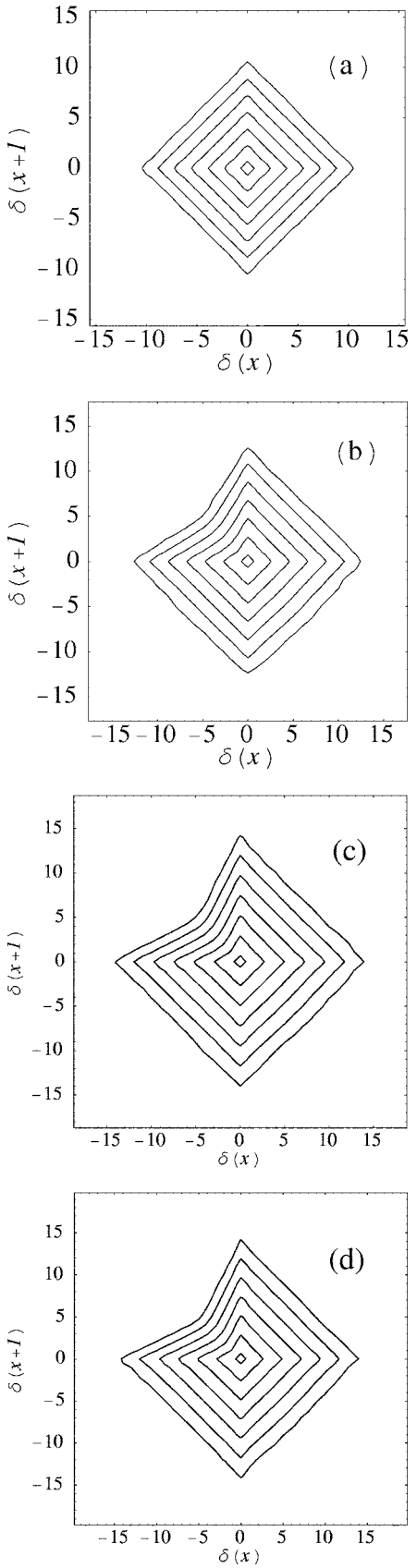

FIG. 14. Contour plots of $\log_{10}p[\delta(x),\delta(x+1)]$ for $\phi=0$ at $T=0.6T_c$ for the OSD dynamics. (a) $H/J=0$. (b) $H/J=1.0$. (c) $H/J=2.0$. (d) $H/J=2.5$. See discussion in the text.

$\delta(x+1)$ (sharp valleys). For weak fields, the TDA shows a weak skewness of the opposite sign, as seen in Fig. 13(b). For the OSD dynamics, for all nonzero fields, the shapes are concave in the second quadrant, Figs. 14(b)–14(d). This shape indicates that large negative $\delta(x)$ tend to be followed by smaller positive $\delta(x+1)$ (rounded valleys). For both dynamics the field dependence in the fourth quadrant, corresponding to the shape of "hilltops," is much weaker that in the second quadrant. As expected, the contour plots for interfaces with $\phi=0$ are always symmetric about the line $\delta(x+1)=-\delta(x)$ for both dynamics.

V. DISCUSSION AND CONCLUSIONS

In this work we have continued our studies of the microstructure of an unrestricted SOS interface driven far from equilibrium by an applied field. Previous studies indicate that different dynamics can lead to important differences in the microstructure of the moving interface and that extreme care therefore must be taken in selecting stochastic dynamics appropriate for the specific physical system of interest.[7–10]

For this study we have considered two dynamics that include a local energy barrier representing a transition state inserted between the individual Ising or lattice-gas states. Such Arrhenius dynamics, as they are often called, are appropriate in kinetic MC simulations of discrete Ising or lattice-gas models in which the discrete states serve as approximations for high-probability configurations in an underlying continuous potential.

The two Arrhenius dynamics that we considered are the commonly used OSD[24,25] and the two-step TDA.[16,17,26] The OSD belongs to the class of dynamics known as soft and the TDA to the class known as hard.[11]

We studied the microstructure and velocity of the SOS interface by kinetic MC simulations and by a nonlinear mean-field theory developed in previous papers.[7,8] We calculated the interface velocity as a function of the driving field, temperature, and angle of the interface relative to the lattice axes. We also studied the local shape of the interface in terms of the spin-class populations, the average height of a step, and the probability density for individual steps in the interface. The theory predicts significant differences between interfaces moving under hard and soft dynamics. For soft dynamics, interface structures should remain independent of the applied field, while there must be a clear dependence on the field for hard dynamics.

For the TDA dynamics we found generally very good agreement between the theoretical predictions and the MC simulations. However, for the OSD dynamics we found that, contrary to the theoretical prediction, there is a weak but clear dependence of the interface structure on the field. This dependence is manifest in the average stationary step height and in the mean stationary class populations, which both show a weak dependence with the field that saturates for strong fields. As a consequence of this dependence, the theoretical results for the velocities do not match very closely the simulated results for low temperatures, particularly for strong fields and small angles.

The interfaces moving under the hard TDA dynamics present similar characteristics to those evolving under a hard Glauber dynamics. However, we found significant differences between the structure of surfaces evolving under the soft OSD dynamics and the soft Glauber dynamics studied in Ref. 9. The velocities under the OSD dynamics present a discontinuity at $T=0$ that is not observed for the soft Glauber dynamics. More interesting is the existence of strong skewness in the OSD model. This indicates that lack of skewness is not a necessary characteristic of soft dynamics, as earlier results seemed to suggest.[9,10]

Within the mean-field approximation used here, individual steps of the interface are assumed to be statistically independent. Short-range correlations are not taken into account by this approximation. The skewness between the spin population on the leading and trailing edges of the interface is a consequence of such short-range correlations. For both the TDA and OSD dynamics, the interfaces undergo a gradual breakdown of up-down symmetry for increasing fields, which has also been observed in other examples of driven interfaces.[31,32,50] This breakdown is clearly evident for the OSD model, and it is probably the reason why the mean-field approximation misses the weak field dependence in the OSD interface structure.

It is obviously important to note and eventually to understand the discrepancies between the theoretical mean-field predictions and the simulation results for the OSD dynamics. However, on a qualitative level the theory predicts quite accurately the differences between the structures generated by the two dynamics. The average step height for the TDA increases dramatically with increasing field, as accurately predicted by the theory. For the OSD, the step height does increase somewhat with H, in contrast to the theoretical prediction of H independence, but the increase is very small. In comparison with the TDA, the OSD surface remains very smooth, with an average step height well below unity.

As in previous studies, our results indicate strong differences between interfaces moving under different dynamics, emphasizing the need for extreme care in selecting the appropriate dynamics for the physical system of interest. Even in cases where soft dynamics are the more appropriate choice, as for solidification or adsorption problems where the driving force is a chemical-potential difference,[12,13,27–29] the results can depend significantly on which soft dynamics are chosen.

ACKNOWLEDGMENTS

G.M.B. appreciates the hospitality of the School of Computational Science at Florida State University. This research was supported in part by National Science Foundation Grant Nos. DMR-0240078 and DMR-0444051, by Florida State University through the Center for Materials Research and Technology and the School of Computational Science, by the National High Magnetic Field Laboratory, and by the Deanship of Research and Development of Universidad Simón Bolívar.

*Electronic mail: buendia@usb.ve
†Electronic mail: rikvold@scs.fsu.edu
‡Electronic mail: kolesik@acms.arizona.edu

[1] *Frontiers in Surface and Interface Science*, edited by C. B. Duke and E. W. Plummer (North-Holland, Amsterdam, 2002).
[2] *Handbook of Heterogeneous Catalysis*, edited by G. Ertl, H. Knozinger, and J. Weitkamp (Wiley, New York, 1997).
[3] D. G. Castner and B. D. Ratner, Surf. Sci. **500**, 28 (2002).
[4] M. Tirrell, E. Kokkoli, and M. Biesalki, Surf. Sci. **500**, 61 (2002).
[5] A.-L. Barabási and H. E. Stanley, *Fractal Concepts in Surface Growth* (Cambridge University Press, Cambridge, England, 1995). Detailed discussion and copious references to the theoretical and experimental literature can be found here.
[6] P. Meakin, *Fractals, Scaling, and Growth far from Equilibrium* (Cambridge University Press, Cambridge, England, 1998), and references therein.
[7] P. A. Rikvold and M. Kolesik, J. Stat. Phys. **100**, 377 (2000).
[8] P. A. Rikvold and M. Kolesik, Phys. Rev. E **66**, 066116 (2002).
[9] P. A. Rikvold and M. Kolesik, J. Phys. A **35**, L117 (2002).
[10] P. A. Rikvold and M. Kolesik, Phys. Rev. E **67**, 066113 (2003).
[11] J. Marro and R. Dickman, *Nonequilibrium Phase Transitions in Lattice Models* (Cambridge University Press, Cambridge, England, 1999).
[12] H. Guo, B. Grossmann, and M. Grant, Phys. Rev. Lett. **64**, 1262 (1990).
[13] M. Kotrla and A. C. Levi, J. Stat. Phys. **64**, 579 (1991).
[14] W. K. Burton, N. Cabrera, and F. C. Frank, Philos. Trans. R. Soc. London, Ser. A **243**, 299 (1951).
[15] S. J. Mitchell, S. Wang, and P. A. Rikvold, Faraday Discuss. **121**, 53 (2002).
[16] T. Ala-Nissila and S. C. Ying, Prog. Surf. Sci. **39**, 227 (1992).
[17] T. Ala-Nissila, R. Ferrando, and S. C. Ying, Adv. Phys. **51**, 949 (2002).
[18] P. Gutlich, A. Hauser, and H. Spiering, Angew. Chem. **106**, 2109 (1994).
[19] J. A. Real *et al.*, Inorg. Chem. **36**, 455 (1997).
[20] M. Nishino, K. Boukheddaden, S. Miyashita, and F. Varret, Phys. Rev. B **68**, 224402 (2003).
[21] M. G. Eilon, Phys. Rev. B **70**, 054404 (2004).
[22] J. D. Muñoz, M. A. Novotny, and S. J. Mitchell, Phys. Rev. E **67**, 026101 (2003).
[23] G. M. Buendía, P. A. Rikvold, K. Park, and M. A. Novotny, J. Chem. Phys. **121**, 4193 (2004).
[24] H. C. Kang and W. H. Weinberg, J. Chem. Phys. **90**, 2824 (1989).
[25] K. A. Fichthorn and W. Weinberg, J. Chem. Phys. **95**, 1090 (1991).
[26] T. Ala-Nissila, J. Kjoll, and S. C. Ying, Phys. Rev. B **46**, 846 (1992).
[27] S. J. Mitchell, G. Brown, and P. A. Rikvold, Surf. Sci. **471**, 125 (2001).
[28] I. Abou Hamad, P. A. Rikvold, and G. Brown, Surf. Sci. **572**, L355 (2004).
[29] I. Abou Hamad, S. J. Mitchell, Th. Wandlowski, P. A. Rikvold, and G. Brown, Electrochim. Acta **50**, 5518 (2005).
[30] M. Kardar, G. Parisi, and Y.-C. Zhang, Phys. Rev. Lett. **56**, 889 (1986).
[31] J. Neergaard and M. den Nijs, J. Phys. A **30**, 1935 (1997).
[32] G. Korniss, Z. Toroczkai, M. A. Novotny, and P. A. Rikvold, Phys. Rev. Lett. **84**, 1351 (2000).
[33] C. N. Yang and T. D. Lee, Phys. Rev. **87**, 404 (1952).
[34] R. K. Pathria, *Statistical Mechanics*, 2nd ed. (Butterworth-Heinemann, Oxford, 1996).
[35] W. Schmickler, *Interfacial Electrochemistry* (Oxford University Press, New York, 1996).
[36] H. Spohn, J. Stat. Phys. **71**, 1081 (1993).
[37] G. H. Gilmer, J. Cryst. Growth **35**, 15 (1976).
[38] A. B. Bortz, M. H. Kalos, and J. L. Lebowitz, J. Comput. Phys. **17**, 10 (1975).
[39] M. A. Novotny, Comput. Phys. **9**, 46 (1995).
[40] P. Devillard and H. Spohn, Europhys. Lett. **17**, 113 (1992).
[41] P. Meakin, P. Ramanlal, L. M. Sander, and R. C. Ball, Phys. Rev. A **34**, 5091 (1986).
[42] M. Plischke, Z. Rácz, and D. Liu, Phys. Rev. B **35**, 3485 (1987).
[43] J. Krug and H. Spohn, Europhys. Lett. **8**, 219 (1989).
[44] J. Kertész and D. E. Wolf, Phys. Rev. Lett. **62**, 2571 (1989).
[45] G. Korniss, M. Novotny, and P. A. Rikvold, J. Comput. Phys. **153**, 488 (1999).
[46] L. Onsager, Phys. Rev. **65**, 117 (1944).
[47] G. M. Buendía, P. A. Rikvold, and M. Kolesik, cond-mat/0512003 (unpublished).
[48] P. Meakin, R. Jullien, and R. Botet, Europhys. Lett. **1**, 609 (1986).
[49] R. Hirsch and D. E. Wolf, J. Phys. A **19**, L251 (1986).
[50] O. Pierre-Louis, M. R. D'Orsogna, and T. L. Einstein, Phys. Rev. Lett. **82**, 3661 (1999).